Characterization of Small Mistuning in a Rotating Bladed Disk Using Stationary Experimental Modal Analysis

Undergraduate Thesis

Presented in Partial Fulfillment of Requirements for Graduation with Honors Research Distinction from the Department of Mechanical and Aerospace Engineering

Karsten Look

Abstract

Bladed disks are of key importance in jet engines and most power generation facilities for exchanging energy with high pressure, high speed flow. These structures are subject to severe vibration which can cause catastrophic failure, motivating the need for accurate modeling techniques. In order to model this behavior, imperfections in components of the system must be measured experimentally. The first part of this study introduces a novel method of stationary modal analysis that is significantly cheaper and faster than current rotating methods. The second part combines the measured data using the Component Mode Mistuning method (CMM) with a Parametric Reduced Order Model (PROM) to predict full system behavior. This study found a strong correlation in measured mistuning values between the two experimental methods, validating the new method. Furthermore, the PROM demonstrated strong computational performance and good accuracy across a wide range of operating speeds. These new methods propose a significant opportunity to reduce the dependency on expensive rotating experiments and allow greatly accelerated design validation capabilities.

THE OHIO STATE UNIVERSITY

COLLEGE OF ENGINEERING

Department of Mechanical and Aerospace Engineering
Under the supervision of Kiran D'Souza
The Ohio State University
March 2020

Contents

List of Figures

List of Tables

Acknowledgments

This work is a component of a very substantial test program running out of the OSU Gas Turbine Laboratory in partnership with Siemens Energy Inc. I greatly appreciate the opportunity to work substantially on both the experimental and computational sides of this project over the past 2+ years.

I would like to thank my faculty advisor Dr. Kiran D'Souza for his assistance in guiding my work at the lab over this time and through the completion of this thesis. I would also like to thank Dr. Randall Mathison for serving on my undergraduate defense committee. On the experimental side I thank Kyle Ruff for giving me the opportunity to assist in many different areas of the lab throughout the construction of the rotating facility. On the computational side, special thanks to Eric Kurstak for the many hours of help and patience teaching me the theory and practice of applied structural modeling in turbomachinery. Starting from a foundational understanding of linear algebra all the way through to a running parametric reduced order model with mistuning corrections, Eric has helped me greatly through the process. Thanks also to the numerous full time staff of the Gas Turbine Lab, and to our technical contact Heinrich Stueer at Siemens. This has been a great opportunity and starting point for my continuing work in turbomachinery.

Chapter 1

Introduction

Gas Turbines are of key importance in demanding applications like aircraft engines and large scale power generation. They require high reliability and have very limited maintenance windows which necessitates a strong understanding of both low and high cycle fatigue to ensure corrective action is taken before life threatening-failure will occur [1].

Fatigue failures occur due to cyclic loading over a long duration, in a bladed disk these are due to vibrations incurred by uneven airflow through the engine, eccentricities in rotating components, and the inherent nature of how air must be guided through the system. A diagram of a bladed disk can be seen in figure 1.1 below. In a perfect system, energy is distributed evenly across all blades of the system and these vibrations have low amplitudes. However, deviations from the nominal design, known as mistuning, can cause energy to concentrate in one or two blades leading to very high amplitudes, high stresses and ultimately shorter lifespan before catastrophic failure.

Mistuning can be large, as in the case of foreign object damage [2][3] or small, due to geometric or material differences. While typically undesirable, mistuning may be intentional [4][5] to balance out other dynamic effects. This thesis will focus on small mistuning, but understanding the sensitivity of the system to small mistuning can potentially address concerns related to large mistuning as well.

This thesis is split into two parts. The first chapter focuses on two methods to experimentally determine small blade mistuning. The first method is a rotating setup [6] that is very time and cost intensive, but can be used for many other investigations outside of determining mistuning properties. The second method introduces a new stationary setup that utilizes an experimental

modal analysis that is several orders of magnitude less costly. This contrasts with optical stationary methods previously introduced by Mabilia et. al [7]. This work culminates in a mistuning pattern of individual blade differences that can then be utilized in a computational model to predict the full system behavior [8].

In the second chapter, the mistuning pattern is integrated into a pristine model of the system and a Parametric Reduced Order Model (PROM)[9] is used to model the full system behavior across a wide range of operating conditions in a computationally efficient manner [10]. Mistuning is added to the PROM in the reduced space using the Component Mode Mistuning (CMM) [11][12] method. The CMM method may also be used to consider multistage systems [13][14][15]. This mistuned model can be used to create predictions to optimize gas turbine designs to increase fuel efficiency, service life, and operational safety.

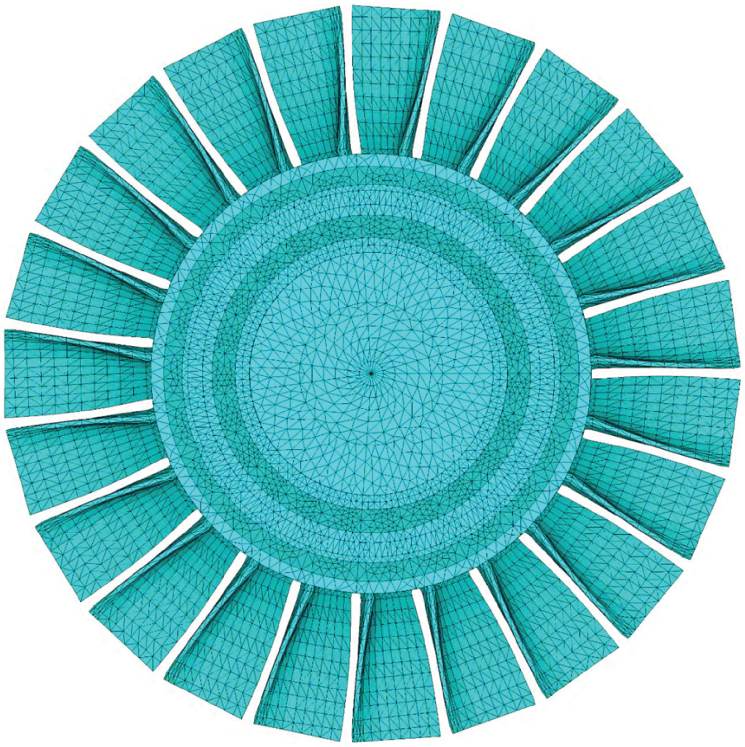

Figure 1.1: Schematic of Bladed Disk

Chapter 2

Experiments

2.1 Theory

Most rigid structures will vibrate when struck; this vibration can be characterized by the frequency at which it vibrates and the mode shape or combination of modes shapes by which it deforms.

The frequency describes the periodicity of the waveform, in the case of a guitar string higher tension in the string will generate a higher frequency vibration that leads to a tone that has a higher pitch. A mode shape is less intuitively familiar, it can be described formally as the specific geometric pattern of deformation that a structure sinusoidally deforms towards at a resonant frequency. More intuitively, a mode shape can be thought of as how a structure naturally tends to deform when it is struck by an impulse. A tuning fork is a structure designed to have a mode shape and associated frequency that is very easy to excite. If one strikes the fork side to side, the primary mode excited has the frequency the fork was tuned to (see fig 2.1). If one strikes it vertically, practically no sound it heard because there are no easily excited mode shapes with associated frequencies in the audible range.

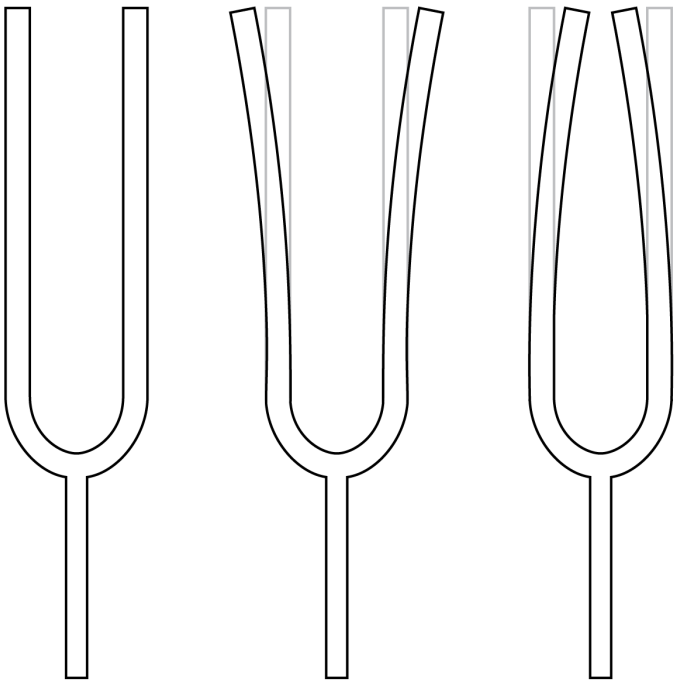

Figure 2.1: The first mode shape for a tuning fork

If an object has a periodic forcing applied, the system is referred to as having a forced dynamic response. If the frequency of the forcing is swept through a given range, the deflection amplitude of the response will peak at certain frequencies. These are known as the resonant frequencies of the system. In a system without damping, forcing at this frequency will generate a response that increases infinitely as the forcing continues. An example would be pushing someone on a swing; there is a specific frequency of pushing that must be met for the person being pushed to increase in swing height. Variations from this frequency will cause the height of the swing to decrease or stay the same. These resonant frequencies are associated with mode shapes to form the modal response.

In most cases, the response of a system is not exactly at a resonant frequency and with a single mode shape, but rather a combination of multiple mode shapes that add together to return the system response. However, knowing the modal responses and how they change with design changes will allow one to make predictions about how the system will respond to any forcing pattern and their associated response. In mechanical systems, the geometry of the object creates a set of modes with frequencies ranging from low values up to infinity, known collectively as the modal response.

In reality, the very high frequency responses are almost never excited and the majority of the response is a combination of lower frequency responses.

When an object is designed, it has a precise geometric and material properties associated with it. However, when it is manufactured it is not possible to manufacture the object to these theoretically perfect specifications. Differences in chemical composition and material processing can change the elastic modulus of the material, which will change the resonant frequency. Small differences the machining process used to form the blades will lead to differences in mass distribution throughout the geometry, this will change the frequency as well as mode shape of the blade. These small variations in geometry and material are collectively known as mistuning, and will change the modal response of the system.

This thesis considers small mistuning, where there is minimal change to the mode shapes and changes can be approximated by only changes in the resonant frequencies for each blade. Over a specified frequency range, the space spanned by the tuned mode shapes matches the space spanned by the mistuned mode shapes; this is a key assumption of the method used to apply mistuning in this study. In contrast, large mistuning encompasses all scenarios in which this assumption does not hold.

The numerous sources of mistuning are lumped together and treated as a single overall blade mistuning, which is assumed be a uniform stiffness through the blade which deviates from the nominal value. Other methods that use multiple parameters [16] or include geometric changes [17][18] have been previously proposed . Mistuning can also affect the structural damping behavior of the system but those effects are not considered for the purposes of this study. While the focus of study of this work is small frequency mistuning, there are significant studies exploring both large mistuning [19][20] and damping [21].

In order to determine the *frequency* mistuning (hereby referred to simply as mistuning), one needs to excite the system into vibrating, then measure how the structure deforms. In the first experiment, the forcing is accomplished with an air jet pointed at the blade, and the vibration is measured by a tip timing system that uses a reflected laser to determine the frequency of vibration. The complexity of the setup stems from the need to rotate the system at operating speeds over 10,000 RPM inside a vacuum chamber, while tracking each blade as it rotates. This measures all blades simultaneously in their operating condition, which gives a direct measure of how the system

responds [22].

In the second experiment, forcing is accomplished by a direct strike with an instrumented hammer and the vibration is measured with a capacitive probe. This system tests individual blades not attached to the hub, and in a fixed reference frame. Demonstrating the relation between the stationary mistuning and the rotating mistuning is the main focus of this chapter.

Other methods for characterizing mistuning are outlined and considered in a work by Weber et. al. [23]. Further, statistical methods have been considered whereby the effect of mistuning is considered at the population level as opposed to an individual system as-manufactured [24][20][25].

2.2 Methodology

2.2.1 Rotating Facility

The goal of this study is to capture the system dynamics of the structure itself in a rotating environment. The presence of air introduces significant complicating factors including viscous damping, additional forcing, and recirculating currents. In order to reduce the influence of these secondary effects, the rotating experiment is conducted within a large vacuum chamber.

The facility itself will respond with its own dynamic response. In order to reduce coupling effects from the facility as well as additional responses from components other than the test article, the tank and test stand were carefully designed to have high structural stiffness and peak responses far from the expected response of the rotor.

In order to test the rotor with rotating effects, it is necessary to spin the test article at operating speeds while measuring the response. This requires a non-contact method of both forcing the system and measuring deflection. Air jets are used to provide forcing as the timing and forcing pattern can be precisely controlled, and they present the capability to generate large forces. These have a disadvantage of introducing air into a vacuum environment, so to compensate large vacuum pumps were installed and run continuously to remove the added air. Other methods of accomplishing this involve pizeoelectric excitation, which has been explored by Mabilia et. al. [7] and Laxalde et, al. [26].

An Agilis light probe system provides non-contact measurement of blade dynamics using a series of light probes that measure reflected laser light from passing blade tips. These return precise timing information about blade arrival and departure times at multiple circumferential locations, which can be converted to deflection amplitudes using Agilis c360® Vibration Intelligence software. By calculating the deflection over time, blade frequencies can be found.

The rotor is supported using two large actively cooled bearing blocks, and rotated using a 28 kW electric motor. Instruments mounted to the disk provide health monitoring information during the experiment and signal and power are transferred using a slip ring mounted opposite the motor.

A diagram of the experiment can be seen in figure 2.2.

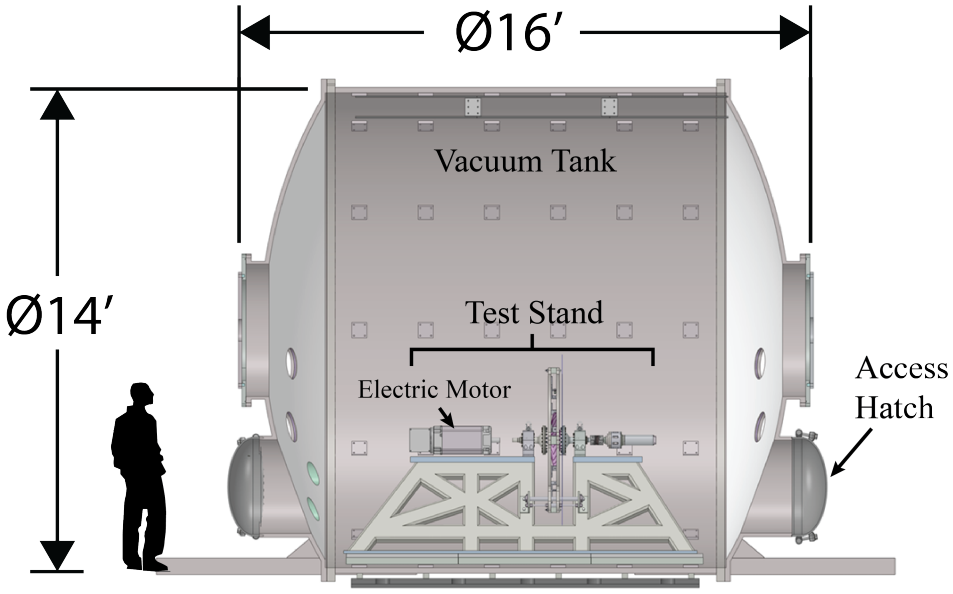

Figure 2.2: Schematic of the rotating experimental facility

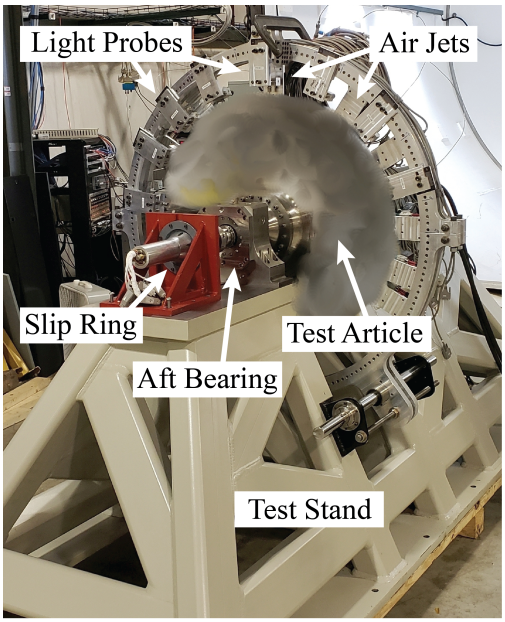

Figure 2.3: Closeup of the test stand

2.2.2 Experiment Conditions

In a rotating system, a stationary air jet in the fixed reference frame will encounter each blade of the rotor at a frequency proportional to the rotational velocity of the rotor. This loading will therefore be inherently periodic and similar on all blades. All blades will deform with the same mode shape and same frequency, the only difference being a phase change between the blades which is proportional to their angular spacing. Nodal diameter is a quantity defined by this phase difference. This is illustrated in figure 2.4 with the signs indicating the direction of deformation relative to the page. One way to excite a specific nodal diameter response is to use the same number of continuous air jets (e.g. To excite a nodal diameter four response, four equally spaced air jets are used).

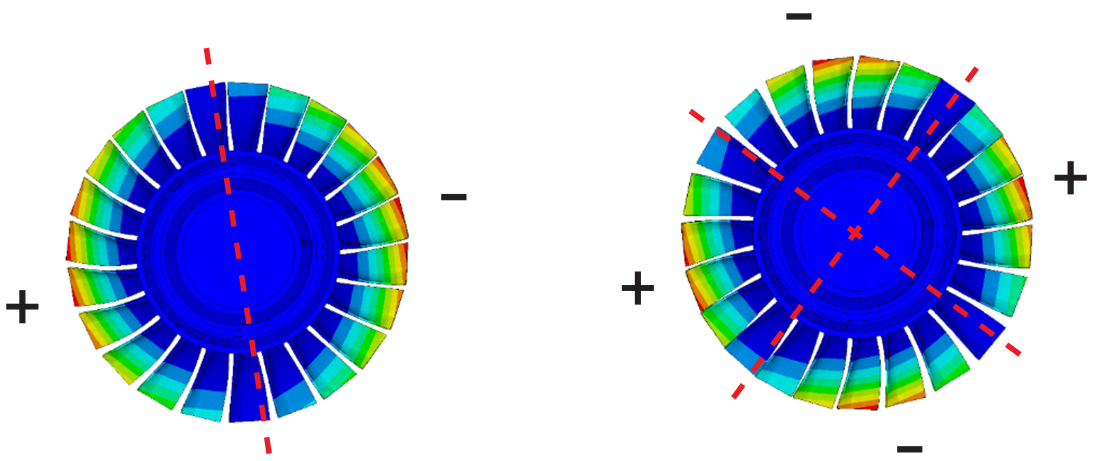

Figure 2.4: Illustration of a nodal diameter one response (left) and a nodal diameter two response (right)

This study focused on a specific set of nodal diameter responses within a given speed range. In a gas turbine, a position upstream of the rotor would house a set of guide vanes that direct flow for maximum energy exchange with the rotor. The number of guide vanes would set the forcing pattern, known as an engine order, which could elicit a corresponding nodal diameter response. The speed range of interest may include areas of atypical behavior or acceleration profiles utilized during operation.

Nodal diameter responses may be categorized as traveling or standing. A standing wave is a

nodal diameter of zero (where all blades are in phase) or N (where N is the number of sectors in the system and is an even number, then each neighboring sector is 180 degrees out of phase with its neighbor). A traveling wave is any other nodal diameter. Traveling waves will propagate around the bladed disk at a fixed wave speed; if the wave speed matches that of the rotation of the rotor turning in the opposite direction the wave will appear stationary to an observer in a fixed reference frame. This is known as a stationary response and is illustrated in figure 2.5. If the speeds do not match, or if the direction of wave propagation matches the direction of rotation then it would be called a rotating response. This is illustrated in figure 2.6.

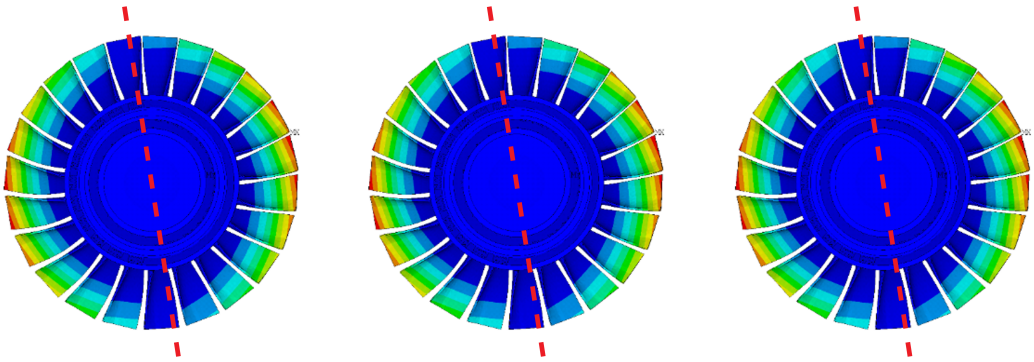

Figure 2.5: Illustration of a stationary traveling wave

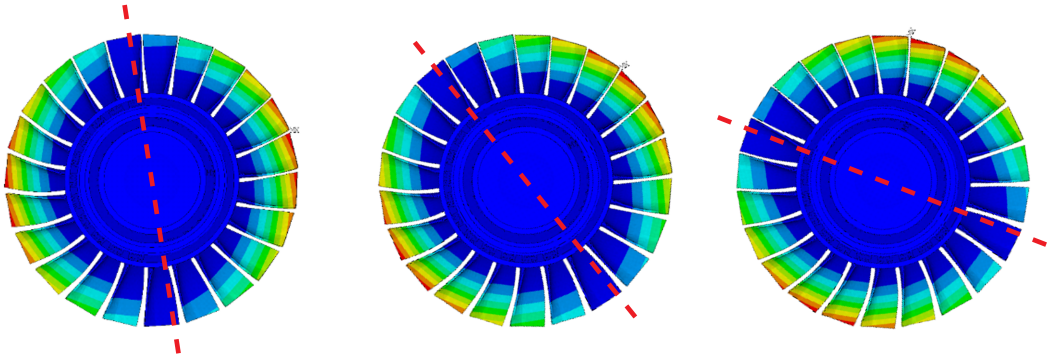

Figure 2.6: Illustration of a rotating traveling wave

This study focuses on a stationary traveling wave for several nodal diameter responses. The stationary waves will be excited by a corresponding number of air jets equally spaced around the circumference of the rotor by means of a support ring.

It is necessary to calculate the speed at which resonance is expected to occur. This is known as the critical speed, and can be calculated by equation 2.1.

$$p_{crit} = 60\frac{f_n}{ND} \tag{2.1}$$

Where p_{crit} is the critical speed in revolutions per minute, f_n is the pristine resonant frequency of the n^{th} mode of interest measured in Hertz, and ND is the nodal diameter of the response.

During the experiments, the rotor was accelerated quickly to a point slightly below the critical speed, then the speed was ramped linearly through the critical speed and slightly beyond to capture higher frequency mistuned responses, this speed profile is shown in figure 2.7. Resonant frequencies for each blade were then found by solving equation 2.1 for frequency.

$$f_{n,mistuned} = \frac{NDp_{crit}}{60} \tag{2.2}$$

Mistuning is then expressed as a zero mean, percentage deviation of the frequency

$$m_n = \frac{f_{n,mistuned} - \bar{f}_{n,mistuned}}{\bar{f}_{n,mistuned}} \tag{2.3}$$

The mistuning pattern is then a collection of the individual mistuning values.

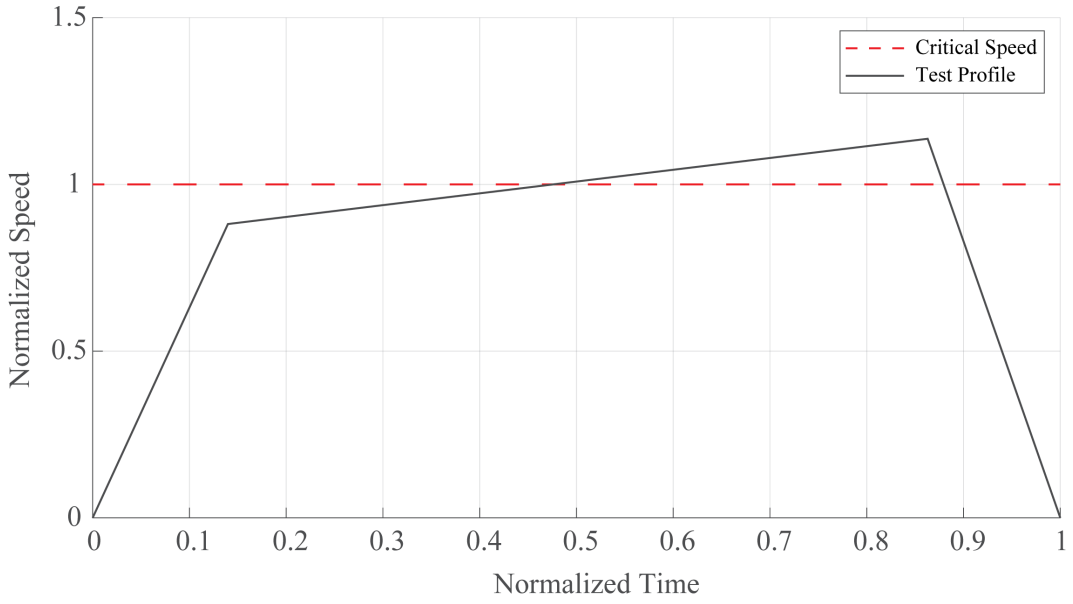

Figure 2.7: Speed profile used in the rotating experiment

It is worth noting that in operation, resonance should be avoided whenever possible. Knowledge of the critical speed should inform design decisions to make the nominal operating speed sufficiently far from resonant conditions in order to maximize rotor lifespan. An operational speed profile is shown in figure 2.8.

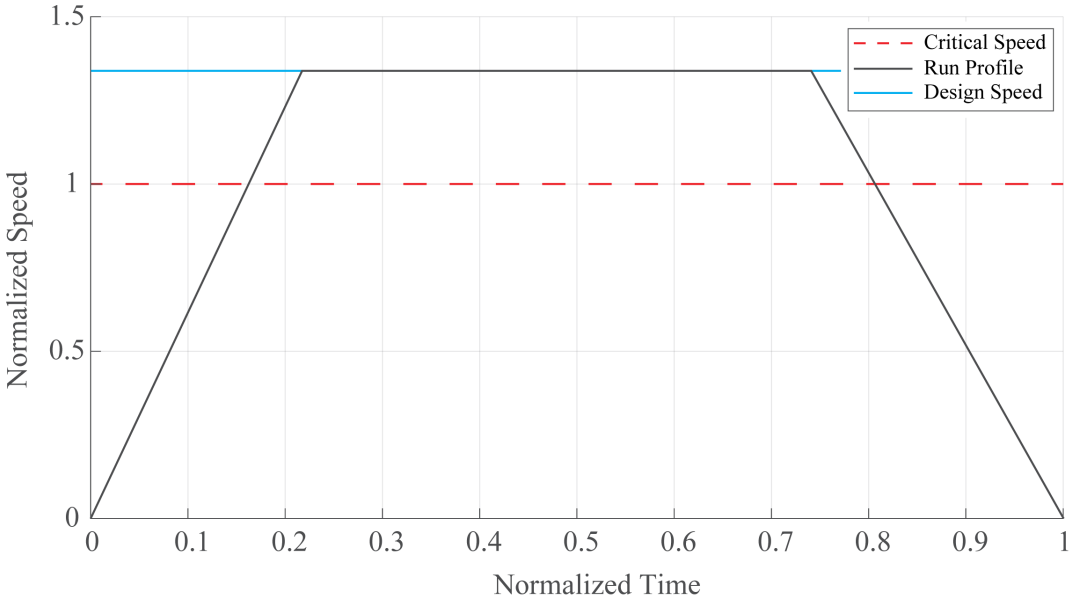

Figure 2.8: Example of speed profile used in operation

2.2.3 Stationary Setup

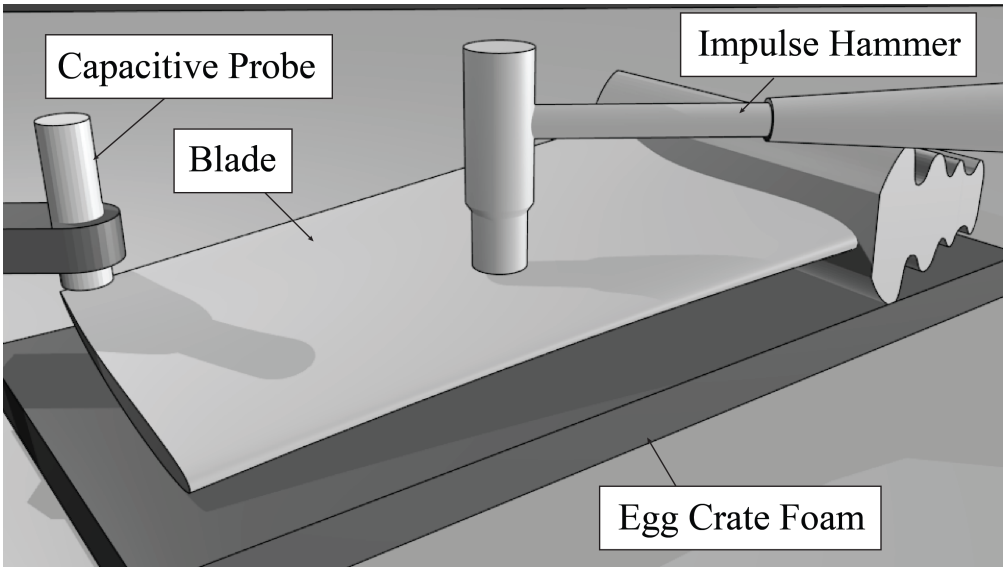

Figure 2.9: Schematic of the stationary experiment

The second set of experiments measured the modal response of individual blades in a fixed reference frame. Egg crate foam was used to isolate the blades from the environment and approximate a free-free boundary condition. Excitation was achieved by using an instrumented impulse hammer to strike the blade at a point of maximum deflection, or antinode, for the first bending mode. A non-contact capacitive probe was positioned at a separate antinode to capture the time domain response. The setup is illustrated in figure 2.9. The antinodes were found by conducting a modal analysis using the pristine blade model. As it was assumed that the mistuned mode shapes do not change significantly, the nodes and antinodes of the pristine blade would approximate those of the mistuned blades.

The stationary mistuned frequencies were calculated by using a Fourier transform to convert the time domain signal into the frequency domain, which is illustrated in figure 2.10. The pristine modal analysis provided an expected tuned frequency that was used as a starting point to locate the correct peak in the experimental frequency data. Several sets of data were collected for each blade, and the average peak value was recorded as the mistuned blade frequency.

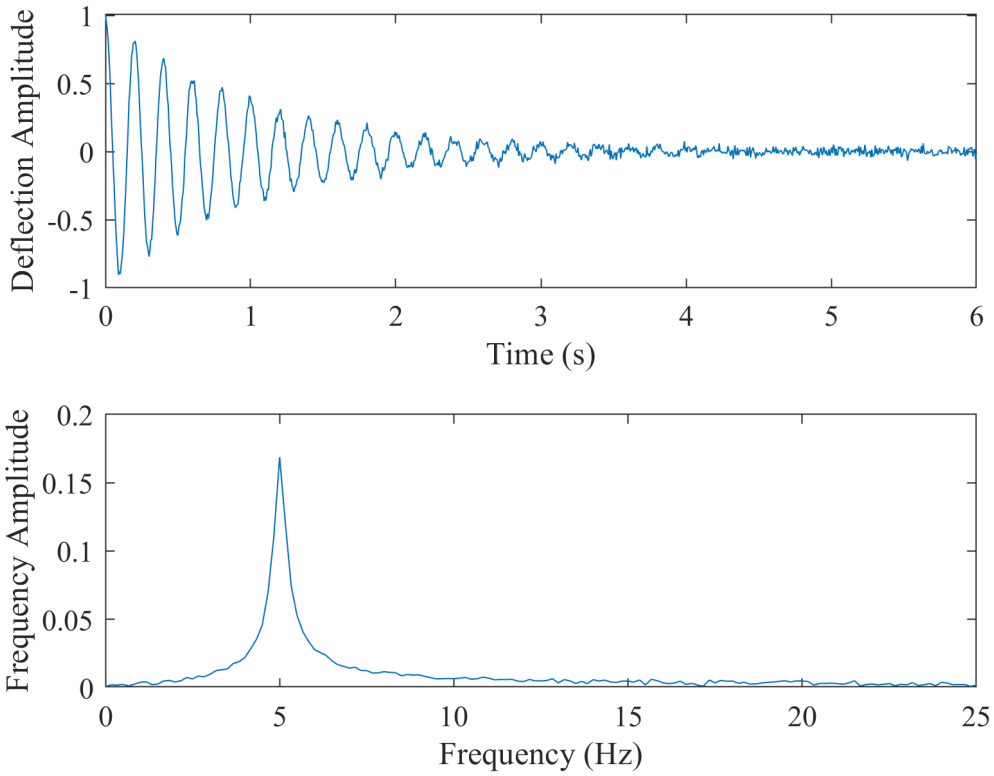

Figure 2.10: A sample of the time domain response (top) and the corresponding frequency domain response (bottom)

It is notable that these experiments were not conducted in a vacuum chamber. While stationary air does introduce additional damping, its effect is small compared to viscous damping in high speed rotating systems. As these experiments are conducted in open air, there is negligible recirculation effects and the blade vibration creates a net zero airflow. Given these assumptions, air damping may be discounted when collecting this frequency mistuning data.

These individual blade frequencies were used to form a mistuning pattern in a similar fashion as described in the previous subsection.

2.3 Experimental Results

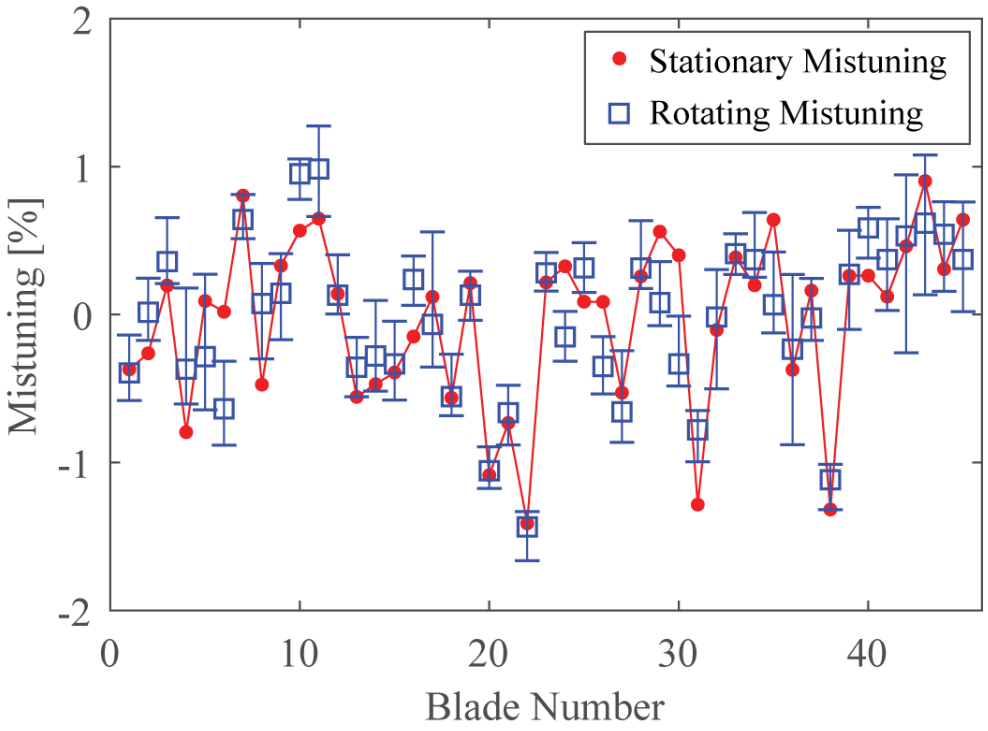

Figure 2.11: Comparison of the stationary and rotating mistuning

Mistuning values found in each experiment are plotted in figure 2.11. The red dots are the percent mistuning found using the stationary experiment, and the blue squares are the average value of mistuning found across multiple experimental runs, with the extreme measurements marked by the limits of the error bars. No error bars were drawn for the stationary measurements, as the greatest deviation of any data set was 0.046% among multiple trials.

The greatest absolute error between the experiments was 0.735%, with the mean absolute error being 0.238%. The data is presented as a zero mean, percent deviation; there is good match of 0.568% and 0.530% standard deviation for the stationary and rotating cases respectively.

2.4 Discussion

Figure 2.11 shows a good match between stationary and rotating values. Some blades demonstrated a large variation in mistuning between the rotating experiments, cause of the variation is currently not well understood. A working theory is that the geometry of the blade root for these blades is inconsistent and that it is experiencing different amounts of contact with the hub, changing the stiffness of these blades at speed. Another potential source of variation is that mistuning values were found while the rotor was accelerating through the resonant frequency. This amplifies uncertainty as few data points are used to determine overall mistuning and non-zero acceleration will add additional system dynamics.

Resonant peaks were determined using a maximum deflection criterion, this may lead to error due to incorrect deflection measurements as the rig and probes themselves vibrate. A method to address this is to instead examine the phase plot and denote the resonant peak at the location at which the phase changes by one hundred and eighty degrees, marking the halfway point of ninety degrees as the point of resonance.

As these experiments are conducted at high rotational velocities, small errors in blade arrival and departure times can have large effects on the observed resonant frequency. Any movement of the rig and probes as well as eccentricity of the rotor shaft or mass imbalance will exacerbate this issue.

Other blades show a greater difference between the two types of experiments. It is well understood that the mode shapes are different between the rotating and stationary conditions due to rotating effects, and the difference between approximated free-free boundary conditions and cantilevered blade boundary conditions. These effects will change the frequencies observed but should affect all blades similarly and so the pattern of difference should be similar. Again individual differences may be explained by differences in blade root geometry on either the blade side or the hub side. Hub deflection effects were discounted as the disk has significantly greater stiffness than individual blades, but it does provide a vector for blade to blade coupling effects to change frequencies further [27].

As the results of the stationary and rotating experiments give similar mistuning patterns, they will result in similar full system behavior predictions when input into the computational model

in the next chapter. The similarity of the data sets indicate that a stationary methodology may be valid for cases of small frequency mistuning, however damping effects will not be captured accurately due to the egg crate foam adding significant artificial damping. The complex contact physics around the blade root while rotating is not well understood, so an accurate stationary damping characterization is currently not feasible.

While the mistuning percentages match between the stationary and rotating experiments, the frequency values cannot be directly compared. There are methods for pre-loading the blade root appropriately to simulate rotational effects [28], however these methods do not capture the stationary stress field effects. Furthermore, blades installed in the disk are not rigidly connected to the structure and depend on centrifugal forces to rigidly lock into position; therefore, a stationary blade-installed comparison is not feasible.

A key benefit of stationary measurements for frequency mistuning is a reduction in facility costs by several orders of magnitude. The rotating experiments required a facility that took approximately two years to construct and multiple millions of US dollars. The stationary experiments may be conducted with much less sophisticated equipment and requires little setup time. Once the facilities are constructed, experiments may be conducted on a similar timescale for both types of setup, however operational costs are still significantly greater for rotating experiments. It is important to note that rotating experiments have significant utility in acquiring other information about the system and should not be discounted.

Another strength of the stationary experiments is the precision with which it returns mistuning values. The greatest deviation in stationary data was orders of magnitude smaller than rotating data, making it an attractive alternative. Validating the accuracy of the stationary mistuning values and their relationship to rotating values is an area of active investigation.

Chapter 3

Computations

3.1 Theory

The results of the previous chapter provide information about blades individually, but a computational model is necessary to predict the full system behavior [29]. There are several complicating factors that must be considered in the methodology.

A primary concern is that the model of the full system is very large, with a single sector of the disk containing over 700,000 nodes with over 2,000,000 degrees of freedom. This results in loading the full system into memory becoming computationally infeasible, much less a modal analysis or time integration. This issue is compounded if multiple test conditions or multiple designs must be evaluated. This motivates the need for a reduced order modeling technique to simplify the model to a tractable size, but it must retain information relevant to the full system behavior. To address changes in operating conditions, a parametric formulation is employed to calculate changes without the need to recompute the full matricies.

The final step requires adding mistuning contributions to the full system. This is not a straightforward process, as mistuning must be applied in the reduced space after parameterizing the matrices. Several operations and corrections are performed to transform mistuning information before forming the final system model.

Structural system dynamics are captured by two independent matrices; the stiffness matrix $\boldsymbol{K}$ and the mass matrix $\boldsymbol{M}$. A third matrix $\boldsymbol{C}$ captures damping and is assumed to be proportional to $\boldsymbol{M}$ and $\boldsymbol{K}$.

3.2 Methodology

The process for forming the computational model consisted of three major steps: determining the blade root contact area, constructing the PROM, and applying mistuning. Determining the blade root contact is a preliminary step in the process. A rotor consists of two main components; the blades which exchange energy with the airflow, and the disk which mechanically couples the blades to the rotating shaft. The contact area between the blades and the disk varies greatly with rotational speed due to changes in the stationary stress field and complex contact physics about the blade root. While a modal analysis can determine information about the blades and disk separately, the contact area must be clearly defined in order to make predictions about the whole system. Subsequent modeling steps utilize this contact area definition to generate pristine system matrices.

The pristine system model is then reduced for computational efficiency. This process discards information not pertinent to the final result such as difficult to excite high frequency modes and specific motion, even at low frequency, that is not of interest. This produces a very dense matrix that is significantly smaller than the full physical system. This may then be analyzed at a feasible computational expense.

When considering high speed rotating systems, it is important to account for two phenomenon that will change the resonant frequencies of the system. The first effect is known as stress stiffening, which is caused by the stationary stress field created by centrifugal forces. It has the effect of increasing the stiffness of the system, thereby increasing the resonant frequency. The other effect is spin softening, which decreases the stiffness and resonant frequency due to radial motion changing the magnitude of centrifugal forces. A representation of these effects is shown in figure 3.1. These effects may be modeled parabolically and applied to the constituent components of the PROM in the reduced space.

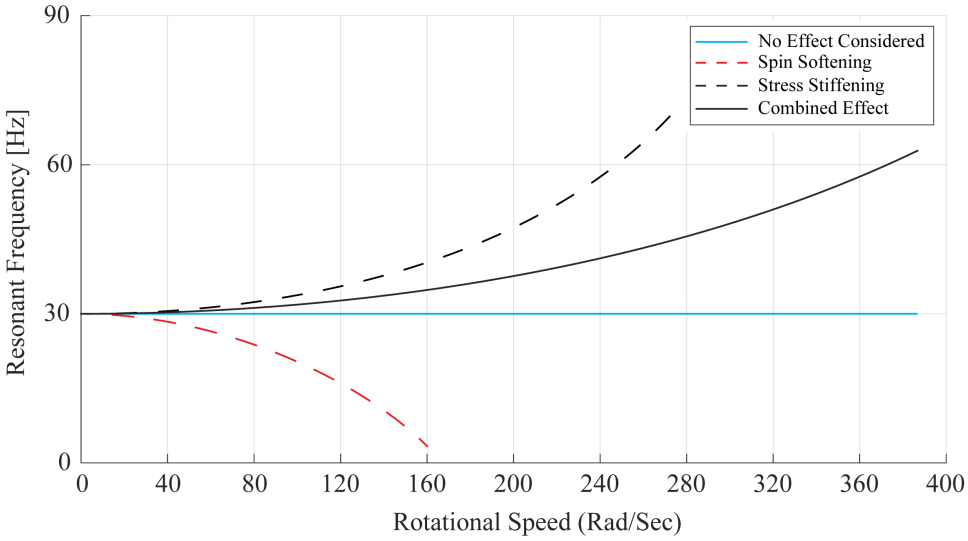

Figure 3.1: Plot of the effects of spin softening and stress stiffening

While the reduction significantly increases analysis speed, the reduction calculation itself is very computationally intensive. A change in operating conditions, such as a speed change, would require recomputing the reduced matrices and a large transformation matrix. This would present a significant issue if the desired quantity were the system response to an acceleration through a critical speed. To address this, the model is parameteterized to enable speed changes to be quickly interpolated for an arbitrary speed in a given range.

The full mistuned system is calculated by adding contributions of the blade mistuning to the parametrically reduced pristine system. This addition occurs in the reduced space, so mistuned physical quantities must be reduced before they may be applied. This has the benefit of decoupling the PROM construction from the mistuning pattern, allowing arbitrary mistuning patterns to be applied at low computational cost. The mistuning must also be parameterized to correspond with the pristine system parameterization. If mistuning were applied without parameterization, rotational effects would be included with the mistuning artificially increasing blade mistuning values as stress field effects increased. To compensate, a corresponding parametric term is used to cancel out rotational effects before mistuning is added to the system.

The resultant matrices represent the system in a compact but highly configurable form. This can be used in many different analyses to produce different predictions about the full system. This

work demonstrates the capabilities by computing the resonant response to a linear acceleration with a constant forcing pattern.

The analyses will be returned in the reduced space, so it is necessary to expand the quantities using the transformation matrix used in the initial reduction to extract physical quantities.

A flow chart for the computational methodology is presented in figure 3.2.

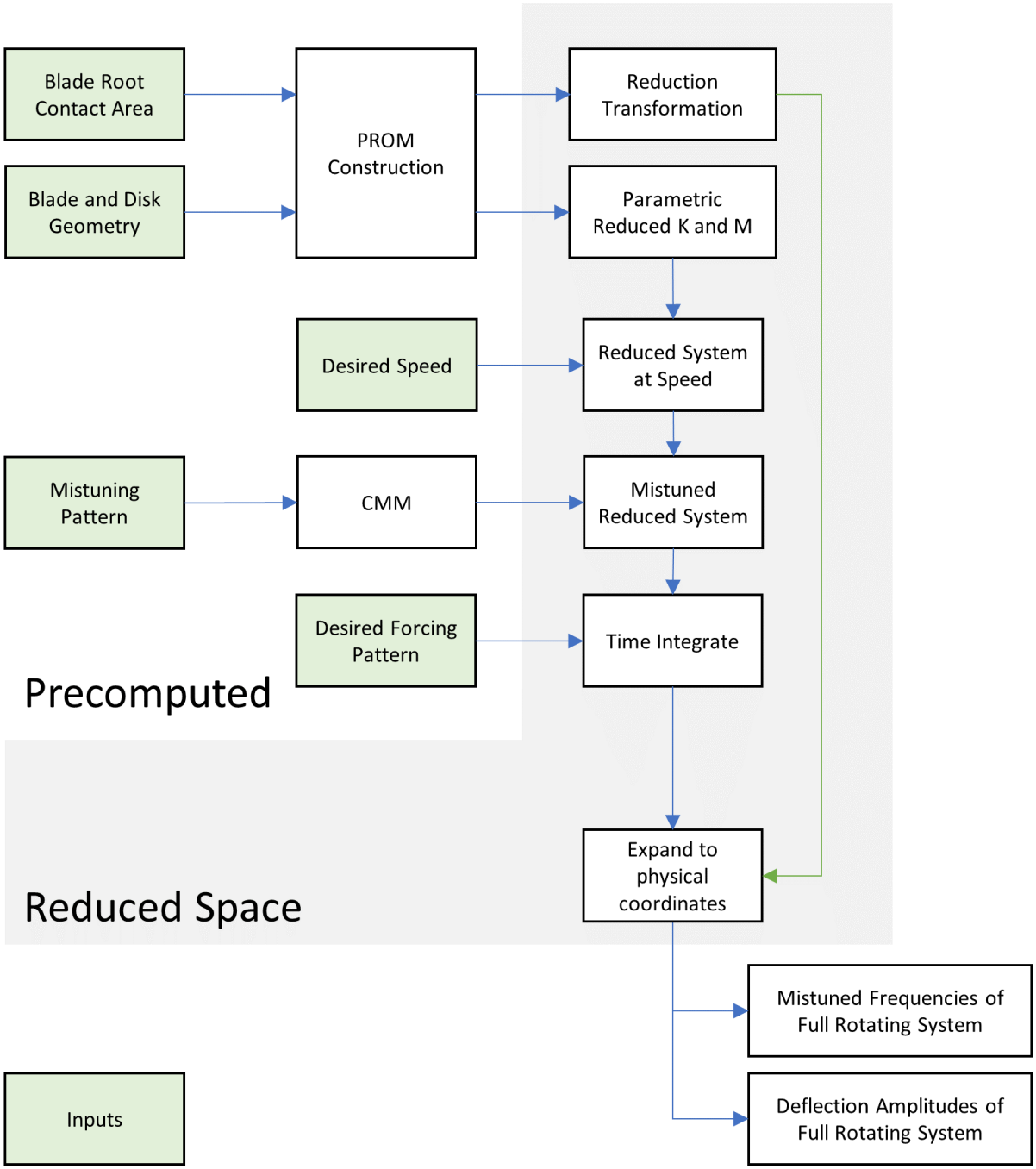

Figure 3.2: Flow chart of computational methodology

3.2.1 Blade Root Contact Area

Blade roots are designed such that contact occurs in a controlled, increasing manner as the rotor increases in rotational speed. This is accomplished by designing the blade root such that a small amount of deformation in either the blade or disk is required before subsequent regions are in contact. Figure 3.3 illustrates such a root geometry. The areas highlighted in red indicate areas in which the blade is contacting the disk slot. The bottom-most regions are first to contact the disk, while the middle regions contact next and the top-most regions contact subsequently.

As contact area increases, the effective stiffness of the blade increases. This is due to the disk possessing significantly higher rigidity than individual blades; more contact will lead to stronger support from the disk. The increased stiffness will lead to an increased resonant frequency in the blade.

It is important to determine the correct contact, as a modal analysis requires a linear system. While in reality contact will increase with rotational speed, it must be approximated as a constant value. In order to determine the contact area, a-priori knowledge about the rotating experiment was required. Blade-disk contact was defined as a multi-point constraint linking the blade and disk structures, the area of contact for both bodies was varied by splitting geometric faces of the contact region as necessary. In order to tune the contact region, multiple rotating pristine simulations were computed and the frequency of the first bending mode was compared to the mean blade frequency in the rotating experiment. The blade contact area is expected to increase with increasing rotational speed due to small deformation in the blade root and disk slot. A mean contact area was selected to approximate both low speed and high speed operation and frequencies were observed to deviate from experimental values by less than one percent. A more complex contact model with varying area and frictional effects may be an area of future investigation.

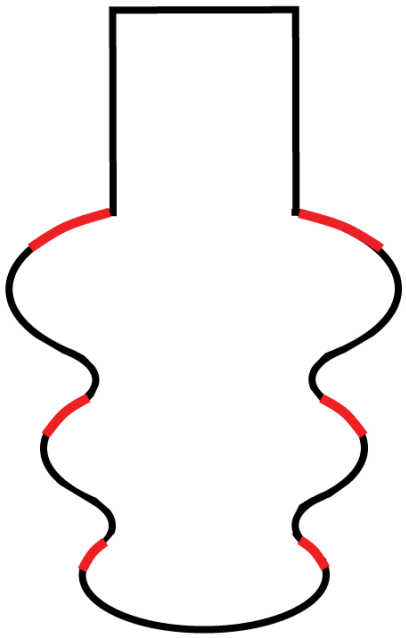

Figure 3.3: Visualization of blade root contact area

In discussion of the practicality of this method, it is feasible that a small number of initial rotating tests may be required to establish the contact region, however this value may be generalized to apply to a large number of simulations. Blade root contact area may stay constant for arbitrary airfoil designs, given that the overall mass and the root geometry is held constant. While it would not eliminate the need for rotating experiments, this method may be used as an exploratory tool in conjunction with rotating experiments to determine regions of interest and perform a preliminary analysis of new blade designs.

3.2.2 PROM construction

Following the contact area definition, a full model may be constructed using Ansys Mechanical. In order to parameterize the system for an arbitrary speed, multiple simulations are required. Rotational effects cause the stiffness matrices to vary quadratically with speed, so three speed points may be used to determine the coefficients to fit a model. A finite difference method is used to determine the correct coefficients, and an assumption of these methods is that the points are equally spaced. It is also important to ensure that the reference speeds selected bound the speeds

of interest, as extended extrapolation decreases model accuracy. For determining resonant behavior encountered during a startup, 0 RPM is necessarily included.

A modal analysis of the system at three equally spaced speeds is then computed and the full matrices saved. To reduce the system, it is necessary to establish a linearly independent set of basis vectors. The mode shapes Φ_p^h at reference speed, p, and harmonic number, h, are compiled into a matrix Φ_{aug}^h

$$\Phi_{aug}^h = \begin{bmatrix} \Phi_{p_0}^h & \Phi_{p_1}^h & \Phi_{p_2}^h \end{bmatrix} \tag{3.1}$$

The mode shapes do not vary significantly with increasing speed, so corresponding mode shapes at different speeds are linearly dependent. A singular value decomposition is calculated and left singular vectors corresponding to singular values less than 0.01% of the largest singular value are removed to ensure a well conditioned transformation matrix.

The final transformation matrix is a compilation of these augmented matricies, allowing the transformation to span multiple speeds and harmonics within a given frequency band.

$$U = \begin{bmatrix} \Phi_{aug}^{h1} & \Phi_{aug}^{h2} & .. & \Phi_{aug}^{h,max} \end{bmatrix} \tag{3.2}$$

This matrix can be used to transform between the physical space and the reduced space. Computationally intensive physical space quantities can be precalculated and reduced, with changes due to speed, mistuning, and forcing computed in the reduced space. This significantly decreases computational expense as the discarded high frequency mode shapes constitute the majority of the matrix size but contribute negligibly to the final solution. Final quantities can then be converted back into physical space by using the transformation matrix.

The stiffness parametrization can then be performed. Quadratically increasing rotational effects may be modeled using the formulation for a quadratic with coefficients determined using numerical methods. From this model, the stiffness at an arbitrary speed may be constructed.

Starting with the equation for a quadratic:

$$ax^2 + bx + c = y$$
$$\frac{d}{dx} \downarrow$$
$$2ax + b = \frac{dy}{dx}$$
$$\frac{d}{dx} \downarrow$$
$$2a = \frac{d^2y}{dx^2}$$

At x = 0:

$$a = \frac{1}{2}\frac{d^2y}{dx^2}$$
$$b = \frac{dy}{dx}|_{x=0}$$
$$c = y(0) = y_0$$

Assembling:

$$y = y_0 + (\frac{dy}{dx}|_{x=0})x + \frac{1}{2}(\frac{d^2y}{dx^2}|_{x=0})x^2$$

Substituting in for x and y:

$$\boldsymbol{K}(p) = \boldsymbol{K}_0 + (\frac{d\boldsymbol{K}}{dp}|_{p=p_0})(p - p_0) + \frac{1}{2}(\frac{d^2\boldsymbol{K}}{dp^2}|_{p=p_0})(p - p_0)^2 \tag{3.3}$$

The terms $\frac{d\boldsymbol{K}}{dp}|_{p=p_0}$ and $\frac{d^2\boldsymbol{K}}{dp^2}|_{p=p_0}$ may be found using a finite difference method centered at the first speed p_0, 0 RPM. It is ccritical that the speeds are equally spaced as this is an assumption of the forward difference formulation.

$$\boldsymbol{K}_{FD}^{1} = \frac{-\boldsymbol{K}_2 + 4\boldsymbol{K}_1 - 3\boldsymbol{K}_0}{2\Delta p} \approx \frac{d\boldsymbol{K}}{dp}|_{p=p_0} \tag{3.4}$$

$$\boldsymbol{K}_{FD}^{2} = \frac{\boldsymbol{K}_2 - 2\boldsymbol{K}_1 + \boldsymbol{K}_0}{(\Delta p)^2} \approx \frac{d^2\boldsymbol{K}}{dp^2}|_{p=p_0} \tag{3.5}$$

Where $\boldsymbol{K}_{p_n}$ is the stiffness matrix at speed p_n and Δp is the difference between reference speeds. K(p) may then be found at an arbitrary speed p by:

$$\boldsymbol{K}_{PROM}(p) = \boldsymbol{K}_0 + \boldsymbol{K}_{FD}^{1} p + \frac{1}{2}\boldsymbol{K}_{FD}^{2} p^2 \tag{3.6}$$

Reducing this quantity with the basis vectors from equation 3.2:

$$\boldsymbol{K}_{PROM}(p) = U^T\boldsymbol{K}^0 U + U^T\boldsymbol{K}_{FD}^{1} U p + \frac{1}{2}U^T\boldsymbol{K}_{FD}^{2} U p^2 \tag{3.7}$$

It is only necessary to transform the mass matrix at one speed as it is constant with rotational speed.

$$\boldsymbol{M}_{PROM} = U^T\boldsymbol{M}(p_0)U \tag{3.8}$$

3.2.3 Applying Mistuning

Mistuning is applied in the reduced space after the PROM is calculated. To avoid double counting contributions from rotational effects the $\delta\boldsymbol{K}$ matrix is quadratically decreased with speed to match the increase in the PROM. This has the net effect of only applying the equivalent blade stiffness changes at all speeds. The compensated stiffness modifications are illustrated in figure 3.4.

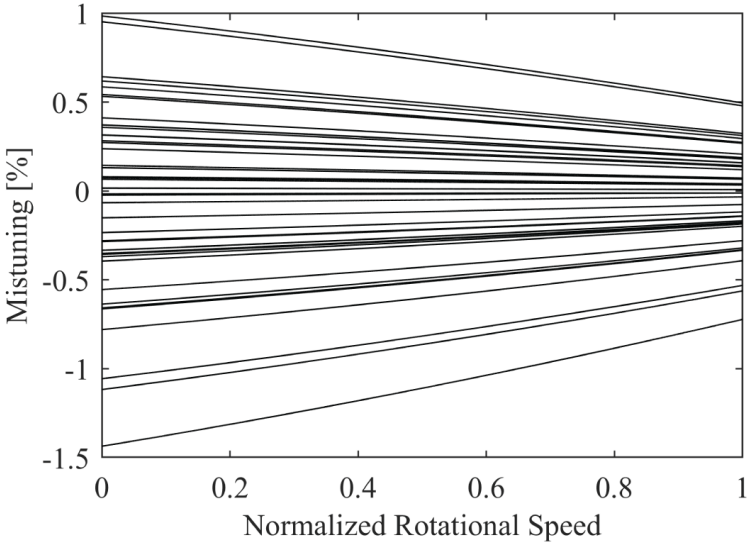

Figure 3.4: Stiffness correction of blade mistuning with speed

A key assumption in the CMM method [11] is that the mistuned mode shapes for small mistuning may be approximated by the tuned mode shapes and only frequency differences are considered when changing the stiffness matrix. Cantilevered quantities are required and may be found by performing a modal analysis on the blade with the disk contact areas held fixed. They are also interpolated as described above using a similar formulation to the PROM speed dependency. The modal participation factors are then used to transform the mistuning values multiplied by the pristine frequencies into reduced $\delta \boldsymbol{K}$ terms.

$$\delta \boldsymbol{K}(p) = \sum_{j=1}^{N} \boldsymbol{q}_j^T(p) m_j(p) \boldsymbol{\Lambda}^{CB}(p) \boldsymbol{q}_j(p) \tag{3.9}$$

Where $\boldsymbol{q}_j(p)$ and $m_j(p)$ are pristine cantilever blade mode participation factors and mistuning values for the j^{th} sector of the disk. $\boldsymbol{\Lambda}^{CB}(p)$ is a diagonal matrix containing the tuned cantilevered blade eigenvalues.

The modal participation factors are then found:

$$\begin{aligned} \boldsymbol{q}_j(p) = & \boldsymbol{\Lambda}^{CB}(p)^{-1} [T^{CB^T} \boldsymbol{K}^{CB,0} T_{PROM,CB,j} \\ & + T^{CB^T} \boldsymbol{K}_{FD}^{CB,1} T_{PROM,CB,j} (p - p_0) \\ & + \frac{1}{2} T^{CB^T} \boldsymbol{K}_{FD}^{CB,2} T_{PROM,CB,j} (p - p_2)^2] \end{aligned} \tag{3.10}$$

Where T^{CB} are the mode shapes of the cantilevered blade, T_{PROM} are the normal reduced modes of the blades in the PROM, and K_{FD} is calculated similarly to equations 3.4 and 3.5. The mistuning values m_j must also be quadratically interpolated:

$$m_j(p) = m_{j,0} + m^1_{FD}(p - p_0) + \frac{1}{2}m^2_{FD}(p - p_0)^2 \tag{3.11}$$

m^1_{FD} and m^2_{FD} are calculated in a similar manner, but as the mistuning does not change at speed, the values for the higher speeds are instead scaled by $\frac{\omega_1}{\omega_0}$ and $\frac{\omega_2}{\omega_0}$ representing how the frequency of the mode changes with respect to rotational speed. The formulas then become:

$$m^1_{FD} = \frac{-\frac{m_{j,0}}{\left(\frac{\omega_2}{\omega_0}\right)^2} + 4\frac{m_{j,0}}{\left(\frac{\omega_1}{\omega_0}\right)^2} - 3m_{j,0}}{2\Delta p}$$

$$m^2_{FD} = \frac{\frac{m_{j,0}}{\left(\frac{\omega_2}{\omega_0}\right)^2} - 2\frac{m_{j,0}}{\left(\frac{\omega_1}{\omega_0}\right)^2} + m_{j,0}}{\Delta p^2}$$

The final stiffness matrix may then be calculated:

$$\boldsymbol{K} = \boldsymbol{K}_{PROM} + \delta\boldsymbol{K} \tag{3.12}$$

This final mass and stiffness matrix was then time integrated using a C++ script and results were transformed back into physical space using the transformation matrix from equation 3.2.

3.3 Results

3.3.1 Contact Area

A crucial first step in forming the computational model was determining the correct contact area between the blade and the disk. This was accomplished by comparing the average mistuned frequency with the pristine frequency given a varying contact area. The results are plotted below and summarized in table 3.1.

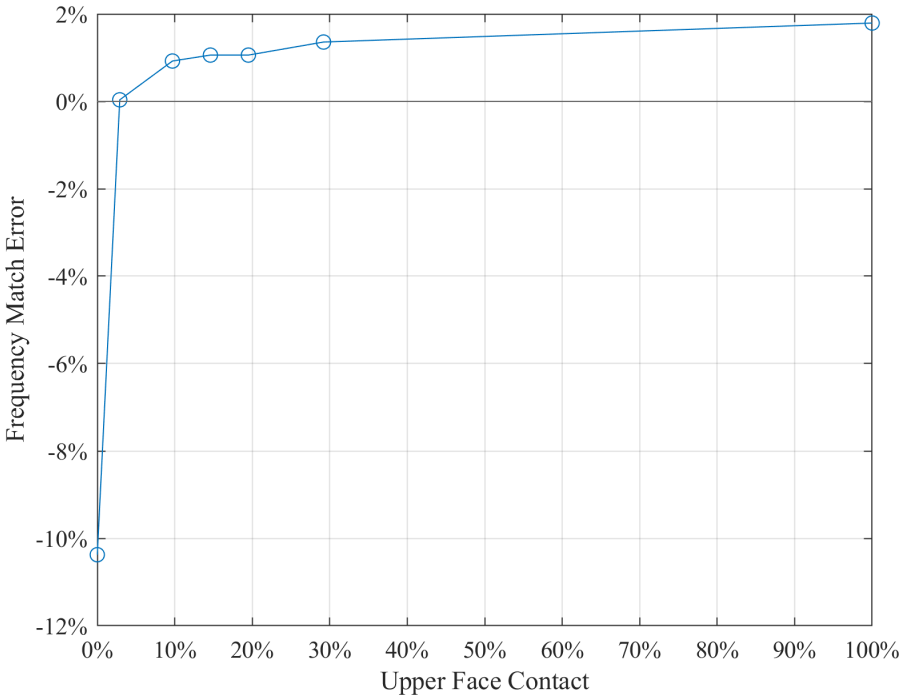

Figure 3.5: Frequency matching error with contact conditions

Upper Face Contact Area (%)	Frequency Error (%)
0	-10.37
2.9	0.04
9.7	0.92
14.6	1.06
19.5	1.06
29.2	1.36
100	1.79

Table 3.1: Table of blade root contact trials

It is observed that the frequency mismatch changed significantly from a no-contact condition to a very small contact of approximately three percent. Subsequently increasing the contact yielded a diminishing increase in frequency. The contact associated with the lowest error of 0.04% was used in the subsequent analysis.

3.3.2 PROM Verification

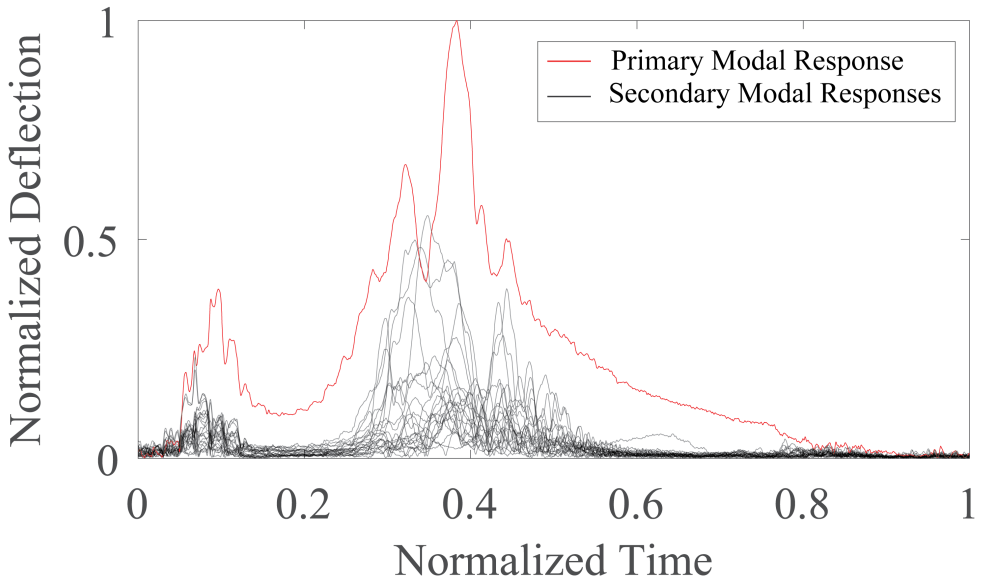

Figure 3.6: Experimental system response with increasing speed

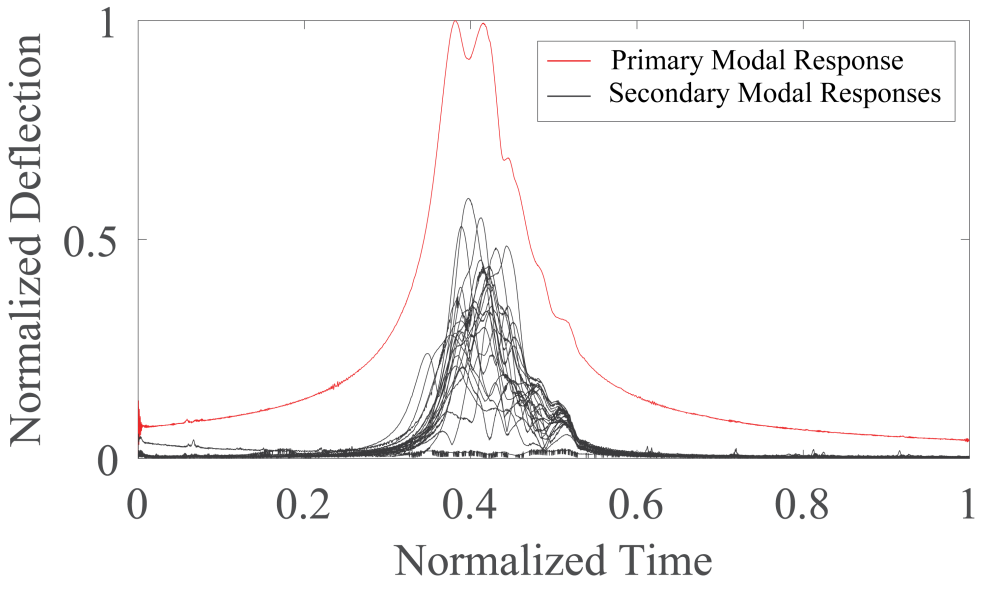

Figure 3.7: Computational system response with increasing speed

Rotating experiments were conducted wherein tip deflection was measured with constant air jet excitation as the speed increased linearly through the expected resonant condition. These results are plotted in figure 3.6. The red line indicates the intended nodal diameter response, while the black lines indicate other nodal diameter responses also excited. In a tuned system with no noise, a single smooth peak would be observed at the tuned resonant frequency. Excitation of other modes occurs due to mistuning and blade to blade coupling effects.

The computational simulation for the same condition is seen in figure 3.7. There is good agreement with predicted peak resonance and the simulation captures secondary modal responses well.

3.3.3 Comparison of blade frequencies

The stationary mistuning values were used with the PROM to generate a full mistuned system. A modal analysis was then conducted on this system and blade frequencies were then compared to the mistuned blade frequencies found in the rotating experiment. This is shown in figure 3.8.

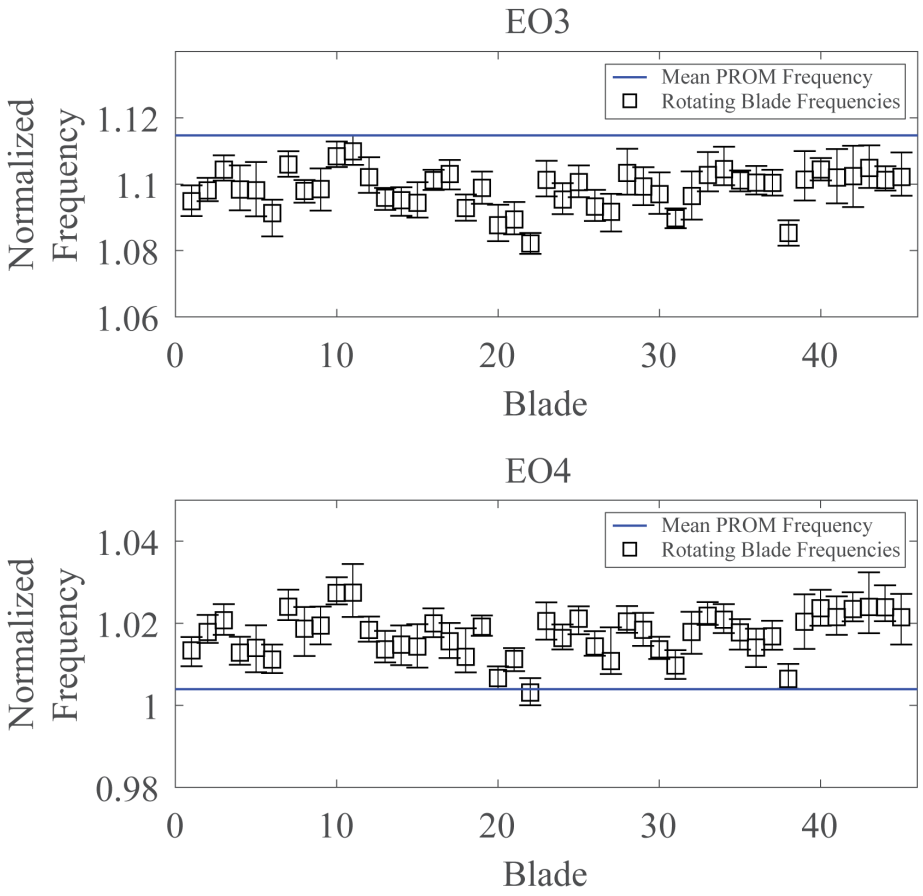

Figure 3.8: Comparison of blade frequencies for nodal diameter three (top) and four (bottom)

The average value from the PROM was within approximately two percent of the experimental values. This indicates a strong performance from the PROM in capturing frequency changes due to rotational effects.

3.4 Discussion

Examining the results of the contact area tuning, the necessity for accurate contact is underscored by the error at the contact extremes. Even the lesser error of two percent at full contact is already larger than the largest value observed in the mistuning pattern. Precision is crucial at this step because the contact definition is required before any full system matrices may be generated. While information from the rotating experiment was required to determine this contact area, a transient simulation that captures the complex contact physics in the root region may be able to determine the value computationally.

In the PROM validation, the experimental plot expressed a small peak in the beginning of the experiment. This occurred due to the air jet system starting at the beginning of the experiment. While it did excite the primary nodal diameter, the response has a low magnitude fast decay as it does not occur at resonant conditions. This startup reading is not present in the simulation as transient startup effects are not of primary concern and were not captured in the initial conditions of the simulation. Notably, there is significantly more noise in the rise to peak deflection in the experimental results. This may be explained by many additional sources of experimental error including electrical noise, vibrations in the rig, laser probes and vacuum tank, and previously discussed errors introduced by the tip-timing system. The computational simulation reflects some mistuning and coupling effects leading to a double peak and some ripple along the falling end of the response.

The match of qualitative resonant shape and quantitative resonant peak indicates that the PROM performed as intended. Strong performance is demonstrated in the ability to capture secondary nodal diameters excited due to mistuning, and the distribution of mistuned amplitudes show good agreement with experimental results. A key strength of this methodology is the ability to simulate many speeds across a substantial time period at a computationally feasible cost.

In the comparison of blade frequencies, the average computational finding for a mistuned frequency fell close to the experimentally derived values. The results demonstrate that while there is room for improvement, the PROM was able to accurately capture frequency changes due to rotational effects. Further analysis is required in order to compare blade by blade predictions and experimental results.

Chapter 4

Conclusions

In the first half of this study, a novel approach to experimentally characterize blade frequency mistuning was introduced. The method demonstrated strong agreement with rotating methods with several orders of magnitude less facility cost. Furthermore, the stationary method returned very precise mistuning values compared to the rotating experiments with the majority of values falling within the range of equivalent rotating results.

While it may not eliminate the necessity for rotating experiments, this method demonstrated strong capabilities to be used as a low cost preliminary analysis tool before significant experimental resources are invested in a design. Furthermore this tool may be used to conduct broader studies particularly in determining manufacturing tolerances and process refinement.

The mistuning data collected from experimental investigations were then used to inform a full system computational model.

In the second half of this study, a full system response was obtained using a computational model. This model demonstrated strong predictive capabilities for both the primary nodal diameter response and secondary responses. It utilized parametric reduced order modeling and component mode mistuning to simulate the complex bladed disk system under a wide spectrum of operating conditions at low computational cost. These significant speed gains were realized by enabling the large full system quantities to be pre-computed and reduced before applying mistuning, forcing, and speed effects. All changing quantities and analysis work was computed in the reduced space after which results could be transferred back into the physical space. As mistuning was applied in the reduced space, arbitrary mistuning patterns may also be applied at low computational expense

enabling statistical studies to examine the system's sensitivity to small mistuning. This may be used to improve design robustness and inform manufacturing tolerances.

Some a priori information about the rotating experiment was needed to construct the model. While this is a current limitation of the work, several possible solutions to address the weakness are presented and show a strong potential line of continued investigation. Furthermore, information gained from initial rotating experiments may be generalized to many operating conditions or multiple airfoil designs. Again, this is a promising line of continued investigation.

The ability to perform analysis very efficiently allows for a very significant number of simulations to be calculated in a feasible time span, enabling faster design iteration and reducing the dependency on intermediary fabrication and physical testing. This may be integrated with optimization tools to generate new designs and explore a more significant design space. This could dramatically decrease development costs while increasing the overall design quality.

Chapter 5

Recommendations

There are several areas of continuing work identified in conducting this study. First, it would be highly beneficial to reduce the need for any physical testing in order to construct the PROM. Work creating a contact model and transient simulation would be a priority avenue for continued investigation.

Further investigation is warranted in determining the source of wide variations in rotating mistuning values. While this work presents several theories, the mechanism is still not well understood and improvements in this area may serve to better validate the stationary experiments as well as provide better input information for the PROM.

Last, introducing tip timing errors and other experimental sources of noise into the simulation may provide a way of better matching the results of the computational and experimental resonant response. In addition to validating the computational methodology, it may serve to inform what areas of improvement would best benefit the experimental data quality and direct further future resources accordingly.

Bibliography

[1] S. Garcia and M. Haag, "Southwest airlines engine explodes in flight, killing a passenger," April 2018. Online.

[2] K. D'Souza, T. Lyons, T. Lacy, and K. Kota *FAA*, vol. Volume IV: UAS Airborne Collision Severity Evaluation: Engine Ingestion, August 2017.

[3] R. A. Michael, "Keep your eye on the birdie: Aircraft engine bird ingestion," *Journal of Air Law & Commerce*, vol. 51, 1986.

[4] M. P. Castainer and C. Pierre, "Using intentional mistuning in the design of turbomachinery rotors," *AIAA Journal*, vol. 40, No.10, October 2002.

[5] R. Corral, J. Beloki, P. Calza, and R. Elliott, "Flutter generation and control using mistuning in a turbine rotating rig," *AIAA Journal*, vol. 57(2), p. 782–795, 2019.

[6] K. D'Souza, E. Kurstak, K. Ruff, and M. Dunn, "Development of an experimental facility for conducting blade damping and mistuning studies at design speed," *AIAA Journal*, 2019. In Process.

[7] A. Mabilia, C. Gibert, F. Thouverez, E. De Jaeghere, L. Sanchez, and L. Giovannoni, "Modal testing of a full-scale rotating woven composite fan using piezoelectric excitation," in *the 10th International Conference on Rotor Dynamics – IFToMM* (K. L. Cavalca and H. I. Weber, eds.), p. 291–305, Springer International Publishing, 2019.

[8] E. Kurstak, R. Wilber, and K. D'Souza, "Parametric reduced order models for bladed disks with mistuning and varying operational speed," *Journal of Engineering for Gas Turbines and Power*, vol. 141(5) 03. 051018., 2019.

[9] A. Sternchüss, *Multi-level parametric reduced models of rotating bladed disk assemblies.* PhD thesis, Ecole Centrale Paris, 2010.

[10] E. Kurstak, K. Look, and K. D'Souza, "Mistuning identification for rotating bladed disks using stationary measurements and reduced order models," in *Proceedings of International Design Engineering Technical Conferences & Computers and Information in Engineering Conference (IDETC/CIE)*, (St Louis, MO, USA), ASME, August 2020.

[11] R. Bladh, M. P. Castanier, and C. Pierre, "Component-mode-based reduced order modeling techniques for mistuned bladed disks - part ii: Application," *Journal of Engineering for Gas Turbines and Power - Transactions of the ASME*, vol. 123, p. 100–108, 2001.

[12] S.-H. Lim, R. Bladh, M. P. Castanier, and C. Pierre, "Compact, generalized component mode mistuning representation for modeling bladed disk vibration," *AIAA Journal*, vol. 45(9), p. 2285–2298, 2007.

[13] S. H. Song, M. P. Castanier, and C. Pierre, "System identification of multistage turbine engine rotors," in *Proceedings of GT2007 ASME Turbo Expo*, ASME, 2007.

[14] K. D'Souza, A. Saito, and B. I. Epureanu, "Reduced-order-modeling for nonlinear analysis of cracked mistuned multi-stage bladed disk systems," *AIAA Journal*, vol. 50, p. 304–312, February 2012.

[15] F. M. Besem, R. E. Kielb, P. Galpin, L. Zori, and N. L. Key, "Mistuned forced response predictions of an embedded rotor in a multistage compressor," *Journal of Turbomachinery*, vol. 138, June 2016.

[16] C. U. Waldherr, P. Buchwald, and D. M. Vogt, "A new mistuning identification method based on the subset of nominal system modes method," *Journal of Engineering for Gas Turbines and Power*, vol. 142, no. 2, 2020.

[17] J. A. Beck, J. M. Brown, A. A. Kaszynski, E. B. Carper, and D. L. Gillaugh, "Geometric mistuning reduced- order model development utilizing Bayesian surrogate models for component mode calculations," *Journal of Engineering for Gas Turbines and Power*, vol. 141, no. 10, 2019.

[18] A. Madden, B. I. Epureanu, and S. Filippi, "Reduced order modeling approach for blisks with large mass, stiffness, and geometric mistuning," *AIAA Journal*, vol. 50, p. 366–74, Feb. 2012.

[19] E. Kurstak and K. D'Souza, "Multistage blisk and large mistuning modeling using Fourier constraint modes and prime," *Journal of Engineering for Gas Turbines and Power*, vol. 140, no. 7, p. 072505– 072515, 2018.

[20] E. Kurstak and K. D'Souza, "A statistical characterization of the effects and interactions of small and large mistuning on multistage bladed disks," *Journal of Engineering for Gas Turbines and Power*, Sept 2019. Accepted.

[21] W. Pastorius, "Damping factors in turbine blade vibration," Master's thesis, University of Windsor, 1969.

[22] D. M. Feiner and J. H. Griffin, "Mistuning identification of bladed disks using a fundamental mistuning model–part i: Theory," *Journal of Turbomachinery*, vol. 126, p. 150–158, March 2004.

[23] R. Weber and A. K¨uhhorn, "Mistuning identification approach with focus on high-speed centrifugal compressors," *Journal of Engineering for Gas Turbines and Power*, vol. 141(3), 2018.

[24] M. Tien, T. Hu, and K. D'Souza, "Statistical analysis of the nonlinear response of bladed disks with mistuning and cracks," *AIAA Jounal, To Appear*, 2019.

[25] K. D'Souza and B. I. Epureanu, "A statistical characterization of the effects of mistuning in multistage bladed disks," *Journal of Engineering for Gas Turbines and Power*, vol. 134, p. 1–8, January 2011.

[26] D. Laxalde, C. Gibert, and F. Thouverez, "Experimental and numerical investigations of friction rings damping of blisks," in *In Proceedings of the ASME Turbo Expo 2008*, (Berlin, GERMANY), p. 469–479, International Gas Turbine Institute, ASME, JUN 2008.

[27] R. R. Craig and M. C. C. Bampton, "Coupling of substructures for dynamic analyses," *AIAA Journal*, vol. 6(7), p. 1313–1319, 1968.

[28] R. Giridhar, P. Ramaiah, G. Krishnaiah, and S. Barad, "Gas turbine blade damper optimization methodology," *Advances in Acoustics and Vibration*, 04 2012.

[29] C. Farhat and M. Geradin, "On a component mode synthesis method and its application to incompatible substructures," *Computers & Structures*, vol. 51, no. 5, pp. 459–473, 1994.

[30] D. L. Gillaugh, A. A. Kaszynski, B. Brown, J. M., J. A., and J. C. Slater, "Mistuning evaluation comparison via as-manufactured models, traveling wave excitation, and compressor rigs," *Journal of Engineering Gas Turbines and Power*, vol. 141(6), 2019.